Contents lists available at ScienceDirect

Journal of Cleaner Production

journal homepage: www.elsevier.com

Fate of pollutants post treatment of acid mine drainage with basic oxygen furnace slag: Validation of experimental results with a geochemical model

Vhahangwele Masindi[a, b, *], Muhammad S. Osman[a], Ryneth N. Mbhele[a], Rirhandzu Rikhotso[c]

[a] Council for Scientific and Industrial Research (CSIR), Built Environment (BE), Hydraulic Infrastructure Engineering (HIE), P.O Box 395, Pretoria, 0001, South Africa
[b] Department of Environmental Sciences, School of Agriculture and Environmental Sciences, University of South Africa (UNISA), P. O. Box 392, Florida, 1710, South Africa
[c] DST/CSIR National Centre for Nano-structured Materials, Council for Scientific and Industrial Research, P.O Box 395, Pretoria, 0001, South Africa

ARTICLE INFO

Article history:
Received 17 January 2017
Received in revised form 21 September 2017
Accepted 16 November 2017
Available online xxx

Keywords:
Acid mine drainage (AMD)
Basic oxygen furnace (BOF) slag
Inorganic contaminants
Neutralization
Geochemical modelling
Recovery of minerals

ABSTRACT

Basic Oxygen Furnace (BOF) slag has been widely used for Acid Mine Drainage (AMD) treatment with its reaction chemistry and contaminants attenuation mechanisms barely reported. This pioneer study was therefore designed with the aim of evaluating the partitioning of inorganic contaminants post the interactions of acid mine drainage and BOF slag and explore the chemistry thereof. This will aid in situation where metal recovery and waste classifications need to be pursued. To fulfil the goals of the study, laboratory experiments were conducted at 60 min of shaking and 100 g: 1 L solids to liquids ratios (S/L). To validate the results, experimental results were complemented by pH Redox Equilibrium (in C language) (PHREEQC) geochemical model. The water chemistry and mineral phase changes during the interaction of BOF and Acid mine drainage (AMD) were evaluated. Reaction of BOF slag and AMD led to an increase in pH (≈10) and a drastic reduction in metal species (≥99%) and sulphate (≥75%). PHREEQC indicated that the removal of chemical species from AMD was dependent on pH. Furthermore, it indicated that Fe was mainly removed as $Fe(OH)_3$, goethite, and jarosite whereas Al was removed as basaluminite, boehmite and jurbanite, $Al(OH)_3$, gibbsite and diaspore. Al and Fe precipitated as iron (oxy)-hydroxides and aluminium (oxy)-hydroxides. Mn precipitated as rhodochrosite and manganite. Ca and sulphate were removed as gypsum. Mg was removed as brucite and dolomite. The results from experimental runs and geochemical modelling were in agreements hence proving that the obtained results are valid. As such, it can be concluded that BOF slag effectively neutralized AMD and significantly lowered the levels of inorganic contaminants to meet prescribed standards as stipulated by the water quality guideline. Gypsum and magnetite were also recovered from mine water treatment process using BOF slag hence depicting that there is commercial value from the treatment process.

1. Introduction

Depending up on the hot metal quality and steel making practice of liquid steel production in a basic oxygen furnace (BOF) slag, for every ton of crude steel produced, approximately 100–200 kg of BOF slag, is generated per ton of steel as by-product, these also depend on the raw material, catalyst and feed been used (Mikhail and Turcotte, 1998; Mahieux et al., 2009). Documented studies have reported that close to 3.9 million-ton of BOF slag is being generated as a solid waste every year from steel industries (Reddy et al., 2006; Belhadj et al., 2012; Chen et al., 2016). This by-product is very heterogeneous and mainly contains large quantity of CaO to flux the oxides of silicon (Si), phosphorous (P), sulphur (S), manganese (Mn) formed during the refining of the liquid steel (Chiou et al., 2006; Chen et al., 2014; Goetz and Riefler, 2014). These oxides combine with the dissolved CaO and form the slag. Fe residues also get incorporated to BOF slag (Chen et al., 2014). After production, BOF slag is partially reprocessed and beneficiated, most steel plants dump this by-product to landfills, BOF retention ponds and lagoons. Beneficiation of BOF slag include: Road construction (Oluwasola et al., 2014), soil amendments (Xue et al., 2006), water treatment (Name and Sheridan, 2014) and metallurgical use (Xue et al., 2006).

On the other hand, South Africa is classified as one of the major producer for coal and Gold globally. Coal is primary used for power generation and for the production of petroleum products where Gold is exported outside the country for further processing (Gitari et al., 2006; Madzivire et al., 2011). Coal has significantly contributed to the power industry in South Africa and Gold has mainly contributed to the Gross Domestic Products (GDP) of the country (Petrik et al., 2003). However, mining of these two valuable products has been reported to impose serious environmental problems (Tutu et al., 2009). This is due to exposure of sulphide bearing minerals during their mining processes (Yesilnacar and Kadiragagil, 2013).

Sulphides bearing mineral exposed during mining activities are prone to react with water and oxygen during rainfall and underground leakages. In most instances, the formation of AMD can be represented by the following chemical equations (1)–(4) (Masindi, 2016):

* Corresponding author. Council for Scientific and Industrial Research (CSIR), Built Environment (BE), Hydraulic Infrastructure Engineering (HIE), P.O Box 395, Pretoria, 0001, South Africa
Email address: VMasindi@csir.co.za, masindivhahangwele@gmail.com (V. Masindi)

https://doi.org/10.1016/j.jclepro.2017.11.124
0959-6526/

$$2FeS_{2(s)} + 7O_{2(g)} + 2H_2O \xrightarrow{bacteria} 2Fe^{2+}_{(aq)} + 4H^{+}_{(aq)} + 4SO^{2-}_{4(aq)} \quad (1)$$

$$4Fe^{2+}_{(aq)} + O_{2(g)} + 4H^{+}_{(aq)} \rightarrow 4Fe^{3+}_{(aq)} + 2H_2O_l \quad (2)$$

$$FeS_{2(s)} + 14Fe^{3+} + 8H_2O \rightarrow 15Fe^{2+} + 2SO^{2-}_{4(l)} + 16H^{+} \quad (3)$$

$$Fe^{3+}_{(aq)} + 3H_2O_l \rightarrow Fe(OH)_{3(s)} + 3H^{+}_{(aq)} \quad (4)$$

These reactions are also mediated by iron and sulphate oxidising bacteria (Eq. (1).) (Doye and Duchesne, 2003; Hallberg, 2010; Akinwekomi et al., 2017). This has led to the formation of a very acidic and metal loaded mine discharges. Due to the nature of a host rock, the mine effluent is rich in sulphate, Fe, Al, Mn and traces of other constituents (Sahinkaya et al., 2009; Sahinkaya and Gungor, 2010; Clyde et al., 2016). For the interest of the public and environmental protection, this mine water needs to be treated prior discharge (Pozo-Antonio et al., 2014).

South Africa has advanced significantly in terms of mine water treatment. Mainly they rely on the use of raw limestone and lime for mine water treatment (Bologo et al., 2012; Maree et al., 2013), this technology has been successfully proven and it is commonly used in mining industries. The only limitation of limestone is partial removal of contaminants from mine effluents and maximum pH of 7. Lime is very effective but cost factor limit its application because it is generated from calcination of limestone (Maree et al., 2013). Moreover, the generated sludge contains hazardous materials that can degrade the environment and pose serious health risk to aquatic and terrestrial organisms.

To minimise the use of virgin materials for mine water treatment and to foster the process of sustainable development, several waste material had to be applied to remediate mine water. Masindi (2016) successfully used cryptocrystalline magnesite tailings for mine water treatment. Name and Sheridan (2014) used metallurgical slags for mine water treatment but they did not explore the chemistry thereof. Other authors also explored the application of BOF slag for mine water treatment (Lee et al., 2016). This study, therefore, attempt to explore the chemistry of BOF slag before and after contacting AMD and the resultant products. BOF slag is rich in Fe and Ca hence making it much easier to recover magnetite and gypsum (Belhadj et al., 2012). Geochemical model will be employed to point out the mineral phases that are likely to form during the interaction of BOF slag and AMD.

2. Materials and methods

2.1. Sampling

BOF slag was collected from a Steel industry in South Africa. Field AMD samples were collected from a coal mine in Mpumalanga Province, South Africa.

2.2. Preparation of BOF slag

BOF slag samples were milled to a fine powder using a Retsch RS 200 vibratory ball mill for 15 min at 800 rpm. Thereafter, it was passed through a 32 μm particle size sieve to get the desired size. The samples were kept in a zip-lock plastic bag until utilization for AMD treatment.

2.3. Characterization of aqueous samples

pH, Total Dissolved Solids (TDS) and Electrical Conductivity (EC) were monitored using CRISON MM40 portable pH/EC/TDS/Temperature multimeter probe. Aqueous samples were analysed using inductively coupled plasma mass spectrometry (ICP-MS) (7500ce, Agilent, Alpharetta, GA, USA).

2.4. Characterization of the feedstocks and secondary sludge

Mineralogical composition of BOF slag and resulting solid residues was determined using X-ray diffraction (XRD). Elemental composition was determined using X-ray fluorescence (XRF), the Thermo Fisher ARL-9400 XP + Sequential XRF with WinXRF software. Morphology was determined using HR-SEM coated with carbon (JOEL JSM – 7500 F, Hitachi, Tokyo, Japan). Mapping, Crystallography and micrographs of cryptocrystalline magnesite were also ascertained using HR-TEM (JEM – 2100 electron microscope, Angus Crescent, Netherland).

2.5. Reaction of BOF slag and AMD

This study will adopt optimum conditions that were reported by the previous studies. For this study, AMD samples were treated at optimized conditions established by a previous studies (Name and Sheridan, 2014; Zvimba et al., 2017). This is a succession study to studies that solely focused on the chemistry of AMD and BOF before and after the reaction. The resultant solid residues after treatment of field AMD were characterized in an attempt to gain an insight on the fate of chemical species. Name and Sheridan (2014) reported that the optimum conditions for remediation of acid mine drainage using BOF slag is 60 min of shaking time and 100 g/1 L S/L ratios. Jafaripour et al. (2015) reported that 15 min was enough for the removal of heavy metals from acid mine drainage using BOS sludge. For the purpose of this study 60 min and 100 g/1 L S/L ratios were used to determine the efficiency of BOF slag for the treatment of AMD.

2.6. Geochemical modelling

To complement chemical solution and physicochemical characterization results, the ion association model PHREEQC was used to calculate ion activities and saturation indices of mineral phases based on the pH and solution concentrations of major ions in supernatants that were analysed after the optimized conditions. Mineral phases that were likely to form during treatment of AMD were predicted using the PHREEQC geochemical modelling code using the WATEQ4F database. Species which were more likely to precipitate were determined using saturation index (SI). In this case, SI < 1 = under saturated solution, SI = 1 = saturated solution and SI > 1 = Supersaturated solution (Parkhurst and Appelo, 1999).

2.7. Quality control and quality assurance

A QC/A programme was established and implemented to ensure the production of trustworthy results. The QC/A process entailed conducting the experiments in triplicate and reporting the data as mean value with Standard deviations (SD). Data was considered acceptable when percentage difference within triplicate samples and percent error were below 10%. The analytical values below detection

limit (BDL) were managed in according to EPA guideline (Wei et al., 2005). The accuracy of the analysis was monitored by analysis of National Institute of Standards and Technology (NIST) water standards. Inter-laboratory analysis was also done to further verify the validity of the results.

3. Results and discussion

3.1. Mineralogical composition of raw BOF slag and the resultant residues

XRD patterns of raw BOF slag (A), synthesized gypsum (B) and recovered magnetite (C) are shown in Fig. 1 below.

The powder XRD pattern of the BOF slag shown in Fig. 1A and it indicates clear peaks of $Ca_2Fe_2O_5$, Fe_3O_4, FeO, $CaFe_2O_4$, $Ca(OH)_2$, Ca_2SiO_4, $[(MgO)_{0.239}(FeO)_{0.761}]$, $CaCO_3$ and Ca_2SiO_5. The formation of Fe_3O_4 is likely to be on account of the oxidation of the entrapped steel in the slag due to water quenching. The more number of humps in the pattern some incomplete crystallization in the slag due to rapid quenching and that the material is very amorphous. The verification of the presence of FeO and Fe_3O_4 was important to assess the magnetite formation mechanism, because Fe^{2+} from these two species contributed to the formation of magnetite through co-precipitation with Fe^{3+} from acid mine drainage. The availability of Ca with aid in the formation of gypsum, this can also be explained by the reduction of sulphate in raw acid mine drainage. After contacting acid mine drainage, there were two fractions of precipitated sludge, the top sludge had high content of gypsum whereas the bottom sludge had high content of magnetite. Fig. 1B the availability of gypsum in the recovered sludge. This is a clear indication that Ca in BOF slag has dissolved and precipitated as gypsum. A clear definition of the reaction chemistry may be defined by the following chemical reactions (Name and Sheridan, 2014):

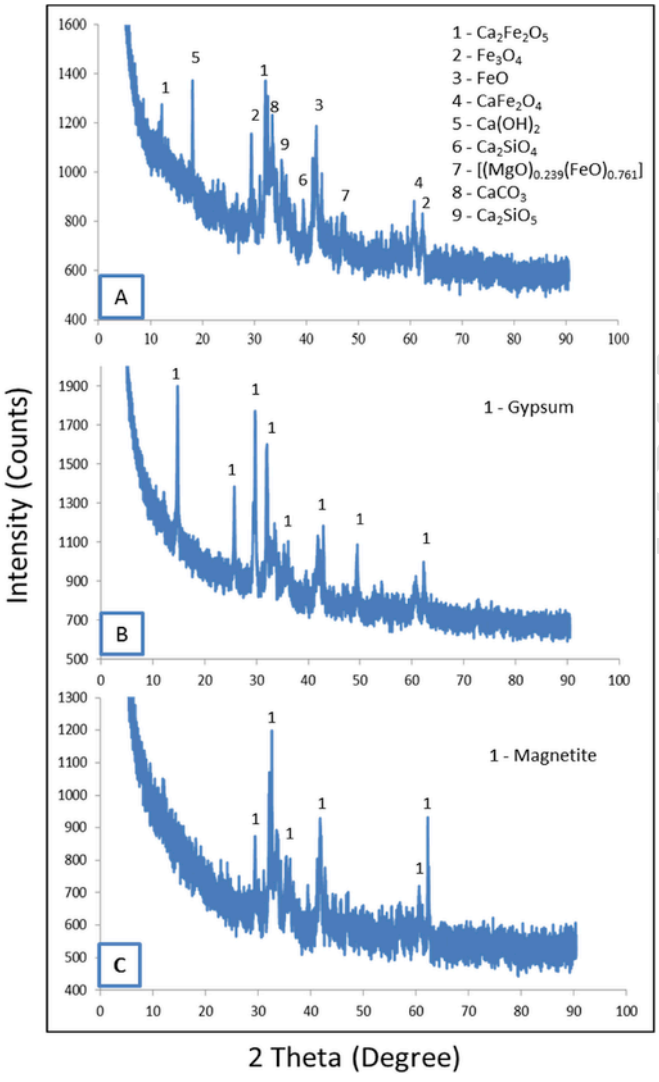

Fig. 1. XRD patterns of raw BOF slag (A), synthesized gypsum (B) and recovered magnetite (C).

$$MgSO_4 + Ca(OH)_2 + 2H_2O \rightarrow CaSO_4 \cdot 2H_2O + Mg(OH)_2 \quad (5)$$

$$CaO + H_2O \rightarrow Ca(OH)_2 \quad (6)$$

$$Ca(OH)_2 \rightarrow Ca^{2+} + OH^- \quad (7)$$

$$Fe^{m+} + MOH^- \rightarrow Fe(OH)_m \quad (8)$$

$$Ca^{2+} + SO_4^{2-} + 2H_2O \rightarrow CaSO_4 \cdot 2H_2O \quad (9)$$

As shown in Fig. 1C, the bottom sludge contained elevated level of magnetite. This may be attributed to high content of Fe in the BOF slag. The chemical reaction occurs during co-precipitation of magnetite from iron salts mixture by raising the pH can be represented as:

$$Fe_2O_{3(s)} + H_2SO_{4(l)} + CaO_s \rightarrow 2Fe_3O_{4(S)} + H_2O + CaSO_{4(S)} \quad (10)$$

or

$$2Fe^{3+} + Fe^{2+} + 8OH^- \rightarrow FeO \cdot Fe_2O_3 + 8H_2O \quad (11)$$

where $FeO \cdot Fe_2O_3$ signifies that the divalent, trivalent iron atoms in BOF slag, $Fe^{3+}/Fe^{2+} = 2$. On rapid raise in the pH, Fe^{3+} ions are immediately precipitated at pH of 3 as highly soluble form Fe-rich mineral phases which then reacts with the existing Fe^{2+} ions in the solution to form magnetite. The XRD patterns shows obvious diffraction peaks corresponding to indices of magnetite at (111), (220), (311), (222), (400), (422), (511), and (440). Similar results of magnetite were reported by (Wei and Viadero Jr, 2007; Rajendran et al., 2015). The position and relative intensity of all the diffraction peaks matched well with the reflection standard of Fe_3O_4.

3.2. Elemental composition of raw BOF slag and the resultant residues

The elemental compositions of raw BOF slag and AMD-reacted BOF slag is reported in Table 1.

As shown in Table 1, the XRF results revealed that the raw BOF slag consist of Ca, Fe, Si, Al, Mg and Mn as major components. Similar results were reported by (Bodurtha and Brassard, 2000; Simmons

Table 1
Elemental composition of raw BOF slag and AMD-reacted BOF slag.

Parameter	Certified	Analysed	Raw BOF slag	AMD-Reacted BOF slag
Wt. %				
SiO_2	99.6	99.70	13.5	11.3
TiO_2	0.01	0.00	0.4	0.3
Al_2O_3	0.05	0.01	7.8	7.6
Fe_2O_3 (t)	0.05	0.01	25.8	28.6
MnO	0.01	0.00	4.4	3.6
MgO	0.05	0.01	7.2	5.9
CaO	0.01	0.01	38.4	29.7
Na_2O	0.05	0.02	0.3	0.2
K_2O	0.01	0.01	0.1	0.05
P_2O_5	0	0.03	1.2	0.9
CoO	0	0.00	<0.001	0.01
Cr_2O_3	0	0.01	0.2	0.1
CuO	0	0.00	<0.001	0.01
NiO	0	0.01	0.01	0.02
PbO	0	0.00	0.02	0.02
SO_3	0	0.00	0.6	9.70
BaO	0	0.00	0.02	0.02
ZnO	0	0.00	0.01	0.04
LOI	0	0.10	−0.2	2
Total	100	99.92	99.7	100.0

et al., 2002; Belhadj et al., 2012; Manchisi et al., 2013; Aziz et al., 2014). Ca was available at elevated concentration as compared to the rest. After contacting the AMD, the level of alkali and earth alkali metals went down hence indicating that there was dissolution of base cations (Name and Sheridan, 2014). Base metals mainly lead to an increase in pH hence precipitating the metals as hydroxide as indicated by equation (12).

$$M^{n+} + nOH^- \rightarrow M(OH)_n \downarrow \quad (12)$$

The obtained results are consistence with the PHREEQC geochemical modelling results. The dissolution of base cations may be represented by the following equations (Masindi et al., 2017):

$$MgO + H_2O \rightarrow Mg^{2+} + 2OH^- \quad (13)$$

$$CaO + H_2O \rightarrow Ca^{2+} + 2OH^- \quad (14)$$

$$Na_2O + H_2O \rightarrow 2Na^+ + 2OH^- \quad (15)$$

This may lead to an increase in the pH of the aqueous system with the subsequent precipitation of chemical species. An increase in pH of the product water may be due to dissolution of traces of silicates as shown by XRD and XRF and the release of Mg, Ca and Na as revealed by XRF and EDS may also contribute to an increase in pH. Silicate will react with acidity in AMD through ion exchange and partial dissolution hence leading to an increase in pH.

$$\equiv SiOH \leftrightarrow SiO^- + H^+ \quad (16)$$

$$\equiv SiOH + Ca^{2+} \leftrightarrow = SiOCa + H^+ \quad (17)$$

$$\equiv SiOCa/Mg + M^{e+} + 2HOH \rightarrow = SiOM + Mg/Ca^{2+} + 2OH^- \quad (18)$$

After reacting BOF slag with AMD, the content of S and Fe went up hence indicating possible attenuation of these chemical species from water. This could better be explained by the resultant water quality.

3.2.1. HR-TEM-micrograph and mapping with EDS of raw BOF slag and AMD-reacted BOF slag

The micrograph and Mapping with EDS of raw BOF slag and AMD-reacted BOF slag using HR-TEM has been reported in Fig. 2.

As shown in Fig. 2, the HR-TEM image of raw BOF slag (A) and AMD-reacted BOF slag (B), indicate the presence of rectangular shaped sachets of hallows to fibre like structures at varying distributional spaces. After contacting AMD, there were changes in microstructural properties of the feed material hence indicting that there was dissolution of matrices from BOF slag. The rod like and spherical deposition were observed on the surface of the secondary residue. This is a clear indication that there were new materials/phases that might have precipitated or adsorbed or co-precipitated onto the sur-

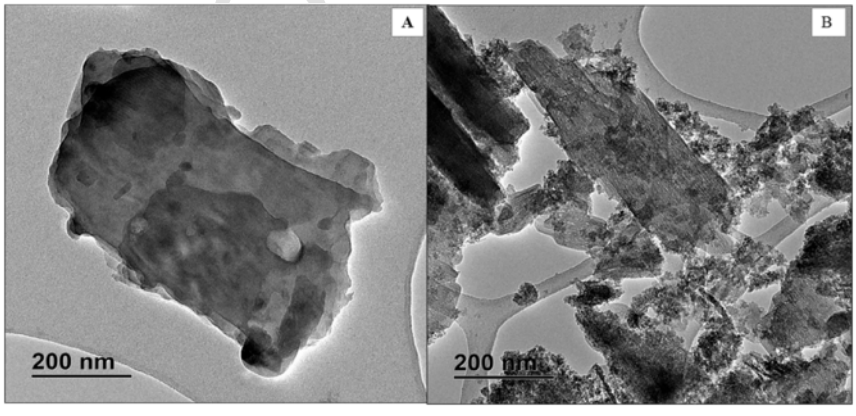

Fig. 2. HR-TEM micrographs of raw BOF slag (A) and AMD-reacted BOF slag (B).

face hence leading to morphological changes. Elemental mapping of raw BOF slag is shown in Fig. 3.

The HR-TEM mapping indicated that the morphology of raw BOF slag is rich in Fe, O, Ca and C. The C is attributed to the grid being used as a platform for TEM. The Ca and O content originate from limestone that is used as a flux. This result conforms to the XRF and XRD results. This will aid in neutralization of acidity and attenuation of sulphate which is the main culprit in AMD. Minute fractions of Al, Mg and S were also observed. Elemental mapping of raw BOF slag is shown in Fig. 4.

The mapping of AMD-reacted BOF slag indicated the different morphologies. The material contained rod like features that are not consistent hence indicating that the material is heterogeneous. The AMD-reacted BOF slag showed the presence of Ca, S and O hence indicating the presence of gypsum ($CaSO_4$). Traces of Mg and Al were also observed.

3.2.2. High resolution scanning electron microscopy (HR- SEM) of raw BOF slag and AMD-reacted BOF slag

The HR-SEM micrographs for raw BOF slag and AMD-reacted BOF slag are shown in Fig. 5.

HR-SEM was used to examine the microstructural properties and morphology of raw BOF slag and AMD-reacted BOF slag. The raw BOF slag (Fig. 5A, C and E) was observed to be heterogeneous and to contain narrow size distribution. There was a difference in texture and morphology from natural aggregates. This was also reported by Xue et al. (2006). The particles were spherical in shape. They also have irregular shapes and coral reef structures and aggregates. The AMD-reacted BOF slag was observed to have sheet and rod-like structures. In addition the surface was crystal smooth hence depicting a typical crystalline shape of gypsum ($CaSO_4$) (Du et al., 2016). Furthermore the rods had different length, ellipsoids and compact surfaces. The surface of the resultant residue was compact indicating that the formed material might be crystalline. The purity of the resultant morphology indicates that there is commercial value in the re-

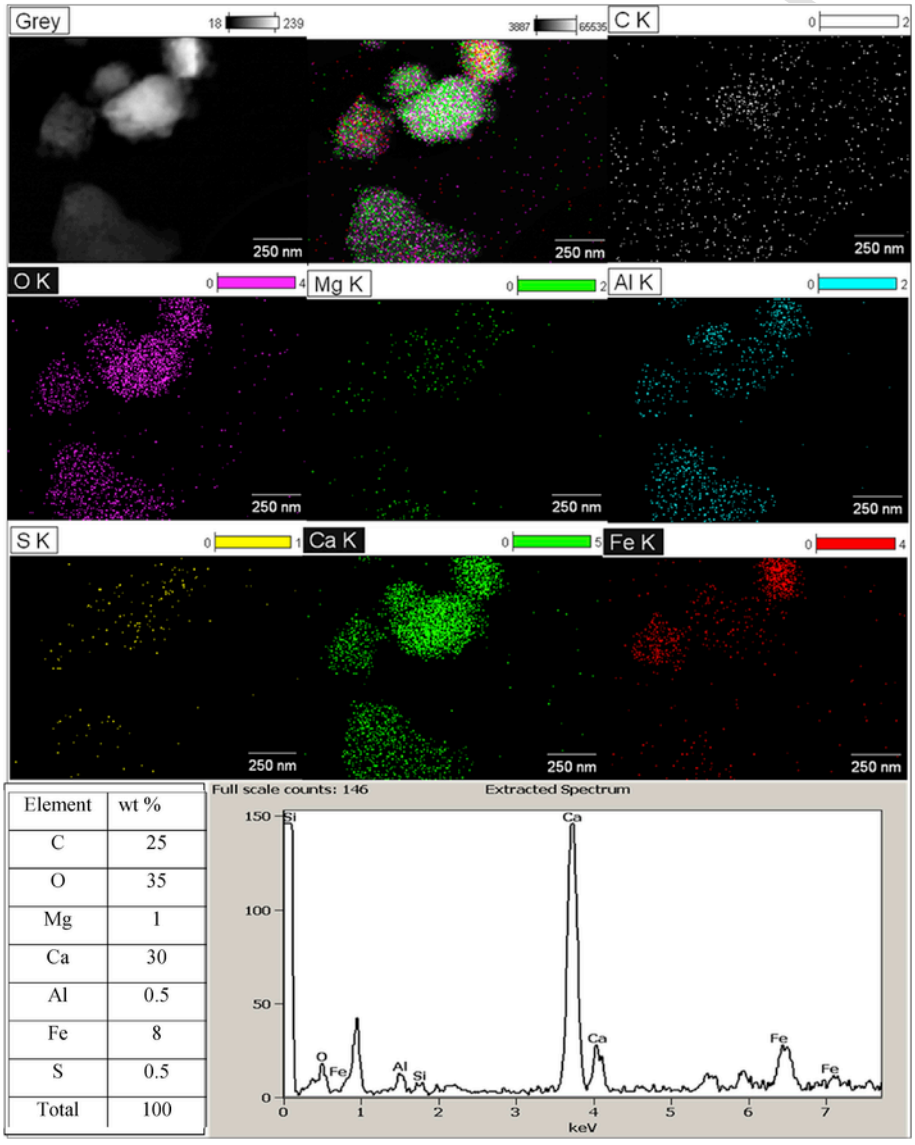

Fig. 3. HR-TEM elemental composition of raw BOF slag.

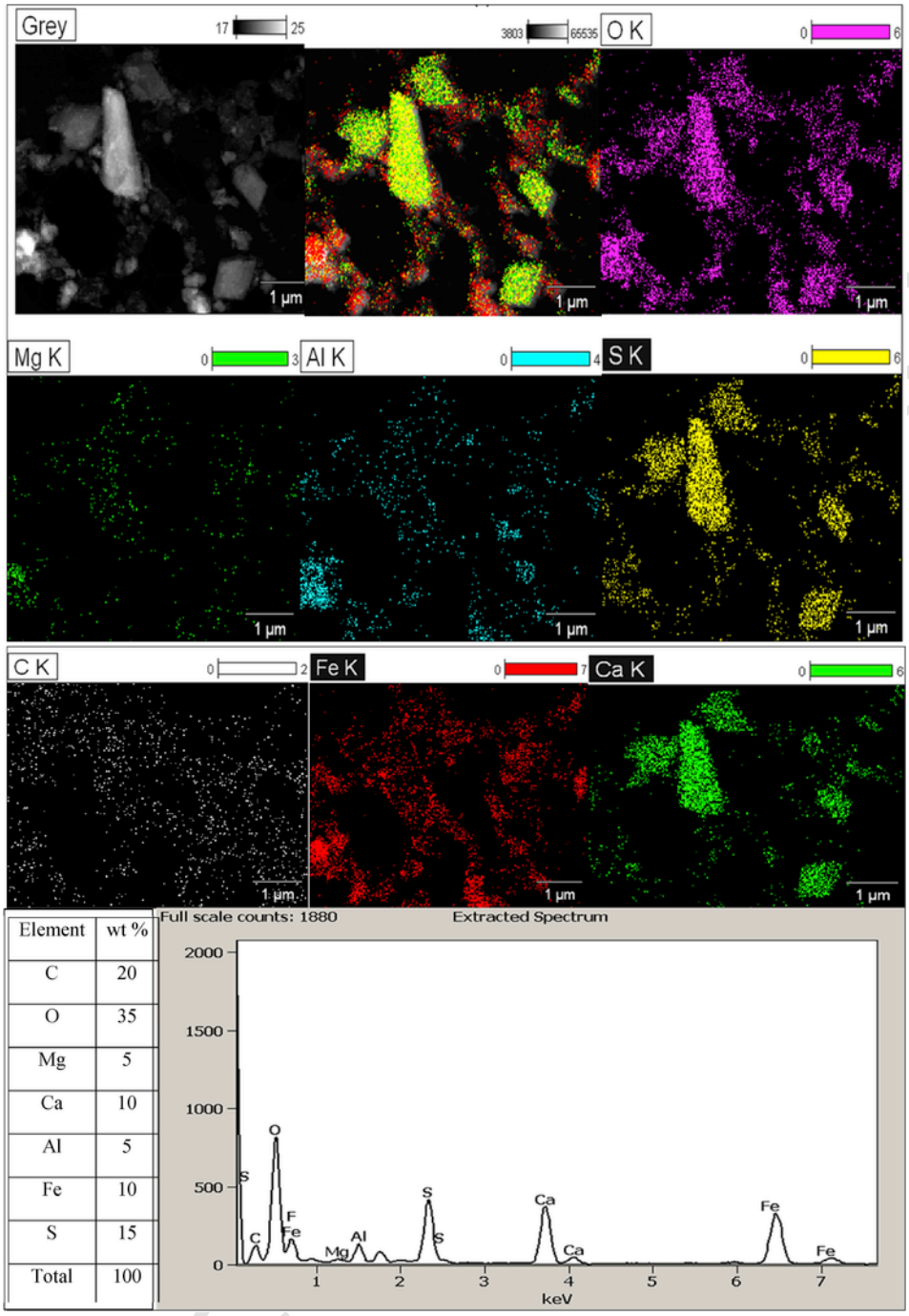

Fig. 4. HR-TEM elemental composition mapping of AMD-reacted BOF slag.

covered material. This indicate the morphological change of BOF slag surface after interacting with AMD hence proving that there was a sink of inorganic contaminants from the solution to the secondary residues. The results of this section corroborate results that were reported by other researchers (Hammarstrom et al., 2003; Du et al., 2016).

3.2.3. HR-SEM of recovered and industrial grade magnetite

The HR-SEM micrographs for recovered and industrial grade magnetite are shown in Fig. 6.

HR-SEM was used to examine the microstructural properties and morphology of recovered magnetite and industrial grade magnetite (Fig. 6). The recovered magnetite (Fig. 6A, C and E) was observed to be heterogeneous and to contain narrow size distribution. The magnetite particles agglomerated into clusters during formation. Similar results were reported by (Wei and Viadero Jr, 2007). The particles were spherical in shape. They also have irregular shapes and coral reef structures. In comparison, the SEM micrographs of industrial grade magnetite particles were partially the same in texture and morphology (Fig. 6B, D and F). This may be attributed to impurities that precipitate with ferrous species from AMD. The crystallinity of the

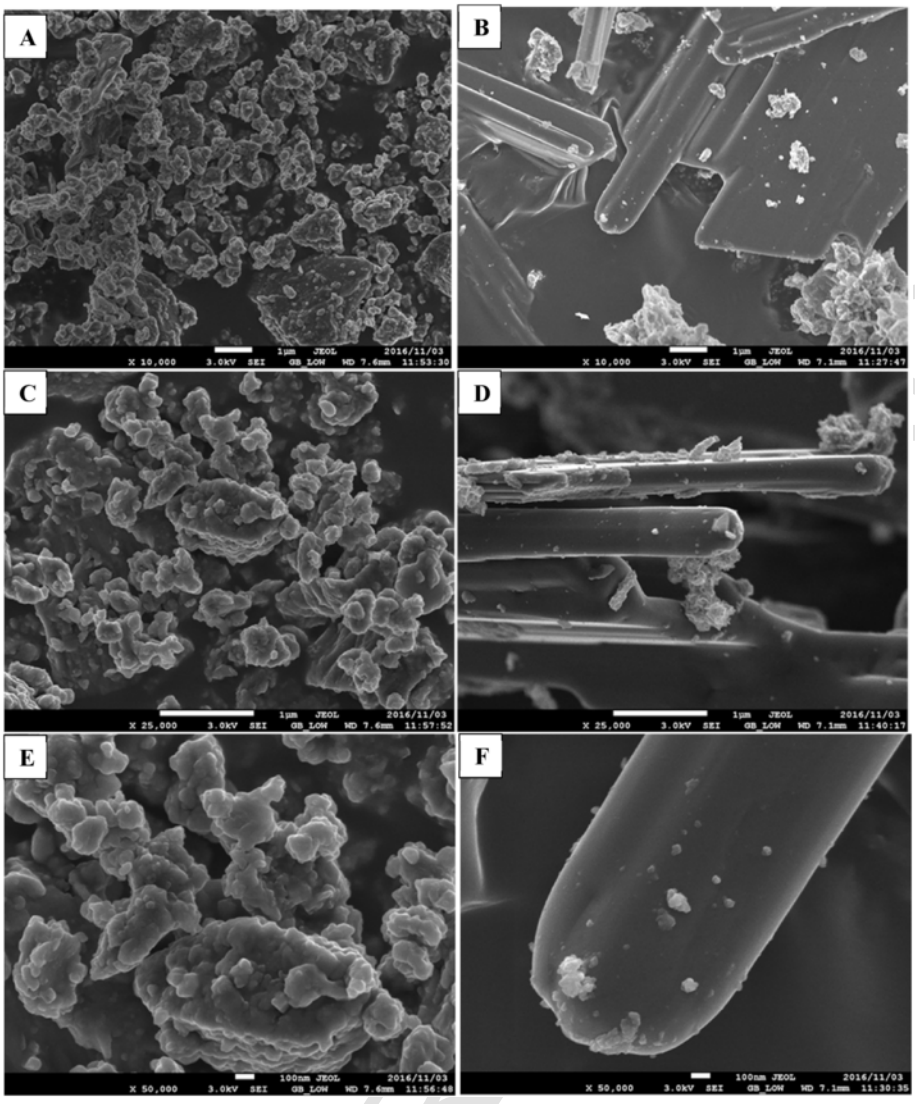

Fig. 5. HR-SEM micrographs for raw BOF slag (A, C and E) and AMD-reacted BOF slag (B, D and F).

two material may also contribute to the slight difference, AMD recovered magnetite (Fig. 6A, C and E) is less compact and smooth than the industrial grade magnetite (Fig. 6B, D and F).

3.3. Modelling of pH and chemical species attenuation at different dosages using PHREEQC

PHREEQC modelled pH and pE of BOF slag reacting with coal mine water is shown in Fig. 7.

Fig. 7 above shows that as the mass increases, pE decreases and the pH increases. This is also evident from the following equation derived from Gibb's free energy:

$$nFE^0 = RTlnK \tag{19}$$

- where, n = no of moles ($n = \frac{mass}{molar\ \ mass}$), F = Faradays' Constant, E° = redox potential, R = gas constant and K = equilibrium constant

Rearranging equation (19) to make E° the subject gives the following:

$$E^0 = \frac{RTlnK}{nF} \tag{20}$$

$$E^0 = \frac{RTlnK}{F} \cdot \frac{Mr}{m} \tag{21}$$

From the equation above, the relationship between mass (m) and redox potential (E°) is inversely proportional. As the mass increases, E° will decrease, and vice versa (Dash, 1994). When the redox potential decreases, the species is then prone to lose electrons. This is because the reduction potential table shows that the more positive the potential, the greater the species' affinity for electrons and tendency to be reduced. For example:

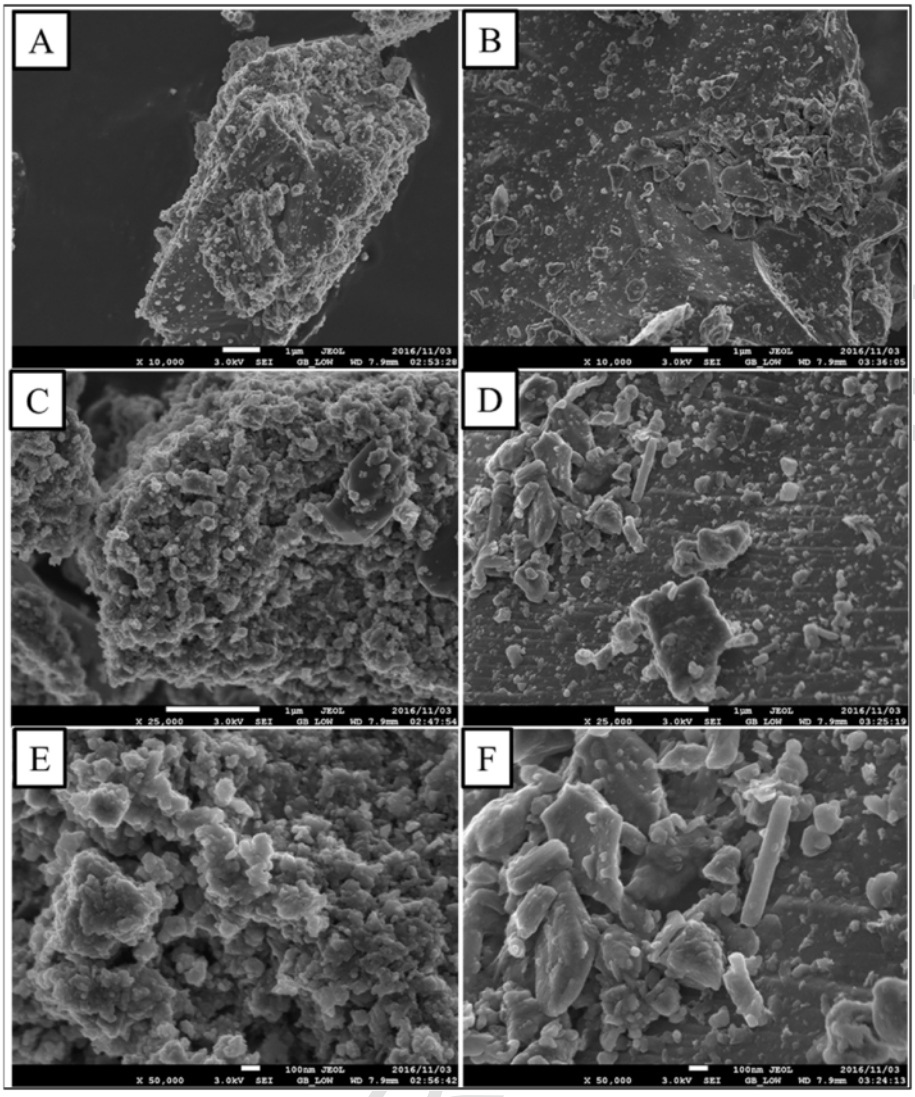

Fig. 6. HR-SEM micrographs for recovered magnetite (A, C and F) and commercial/industrial grade magnetite (B, D and F).

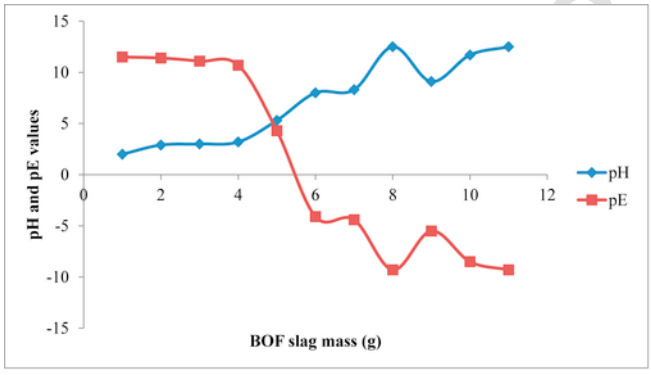

Fig. 7. PHREEQC modelled pH and pE of BOF slag reacting with coal mine water.

$$Zn^{2+}_{(aq)} + 2e^- \leftrightarrow Zn_{(s)} \qquad E^0 = -0.74V \tag{22}$$

$$Cu^{2+}_{(aq)} + 2e^- \leftrightarrow Cu_{(s)} \qquad E^0 = +0.34V \tag{23}$$

Between the above two species, Zn will be oxidised since it has a lower potential, hence losing electrons. Cu^{2+} will be reduced, hence gaining electrons. The half reactions then become:

$$\text{Oxidation half reaction}: \quad Zn_{(s)} \rightarrow Zn^{2+}_{(aq)} + 2e^- \tag{24}$$

$$\text{Reduction half reaction}: \quad Cu^{2+} + 2e^- \rightarrow Cu_{(s)} \tag{25}$$

When pE decreases, pH increases. This is because the solution starts to be more alkaline, hence a decrease in the cations. When the concentration of cations is lower, the pH becomes higher. This is true

by Fig. 6 as well.

At pH = 9.1, $[H^+] = 7.94 \times 10^{-10}$
At pH = 11.7, $[H^+] = 1.99 \times 10^{-12}$
At pH = 12.5, $[H^+] = 3.16. \times 10^{-13}$

At these points of the graph, the solution has high alkalinity. This in turn affects the electrical conductivity (EC) as the metal ions would have decreased in the solution i.e. they have precipitated, hence decreasing the electrical conductivity. PHREEQC modelled chemical species concentration of BOF slag treated coal mine water is shown in Fig. 8.

As shown in Fig. 8. There was a distinguishable relationship between molarity of chemical species in AMD treated with BOF slag and their respective masses. The major elements in the AMD treated with BOF slag are Al, Fe, Ca, Mn, SO_4, Mg and K. Fe and SO_4 were observed to be the dominant species and this communicates very well with the ICP-MS results on water quality. However, after contacting a BOF slag there was a decrease in the concentration of Al, Fe, Mn, and SO_4, was observed hence confirming that there was chemical species attenuation. There was a drastic reduction in Al and Fe with an increase in dosage. K and Cl remained constant in an aqueous system, thus, indicating that they were not removed during the reaction. The obtained results could further be explained by the water quality and the recovered sludge. A reduction in metal species may be attributed to an increase in the pH of a solution with an increase in BOF dosage, hence leading to their respective precipitation (Eqn. (12)). This indicates that the hydroxyl group becomes dominant in the solution, hence increasing the alkalinity of the solution (Eqns. (13) and (14)). The inversely relationship between Ca and SO_4 in the solution depicts the formation of gypsum ($CaSO_4$) which is recovered at the end on secondary sludge. SO_4 decreased with an increase in dosage and Ca content. This indicates that increasing of dosage lead to an increase in Ca content hence reducing the SO_4 as $CaSO_4$. The modelled results corroborate the mineralogical results where gypsum was determined to be present in the secondary sludge using X-ray diffraction. Furthermore, similar results were obtained from X-ray fluorescence where Ca and S were the dominant element in the sludge. ICP-MS also showed a significant reduction in Al, Fe, Mn and SO_4 hence complementing the results obtained from geochemical model.

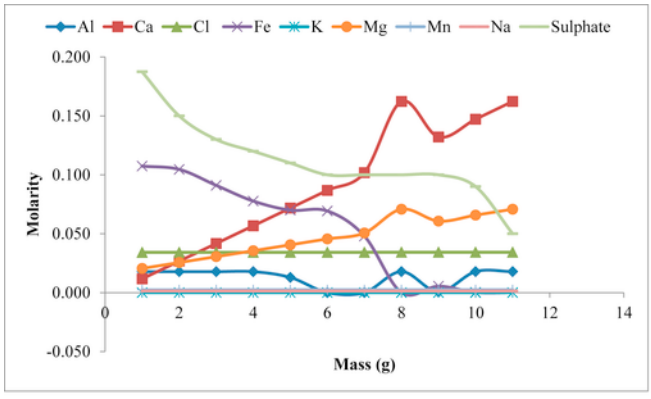

Fig. 8. PHREEQC modelled chemical species concentration of BOF slag treated coal mine water.

4. Prediction of mineral phase precipitation using PHREEQC

The results for calculation of mineral precipitation at various pH during treatment of AMD with BOF slag are presented in Table 2.

The results obtained in this study conform to other results reported in literature (Madzivire et al., 2010; Masindi et al., 2016). Most of the Al and Fe could precipitate as hydroxides at pH > 6. Mn could precipitates as manganese hydroxide at pH > 10 and rhodochrosite at pH > 8. Sulphate-bearing minerals could precipitates at pH 6–8 (basaluminite), pH > 8 (gypsum), pH 6 (jarosite and jurbanite). For example sulphate could interact with those species as follows [Equation (26 - 28) (Masindi et al., 2017)].

$$M^{n+} + nOH^- \rightarrow M(OH)_n \downarrow \quad (26)$$

$$Al(H_2O)_3(OH)_3 + SO_4^{2-} \rightarrow Al(H_2O)_3(OH)(SO_4) + 2OH^- \quad (27)$$

$$Fe(H_2O)_3(OH)_3 + SO_4^{2-} \rightarrow Fe(H_2O)_3(OH)(SO_4) + 2OH^- \quad (28)$$

Generally, mineral phases were predicted to precipitate as metal hydroxides, hydroxysulphates and oxyhydroxysulphates. However, sulphates were removed from solution together with Al, Fe and Ca. This corroborate the SEM-EDS and XRF detected Al, Fe, Mn and S rich mineral phases were deposited to solid residues. This indicates that the Al, Fe, Mn and S rich mineral phases were too amorphous to be detected by XRD or the concentration was below the detection limits. PHREEQC modelled chemical species concentration of BOF slag treated coal mine water Figs. 9 and 10. This will support the results obtained by the XRF and XRD.

From Figs. 9 and 10, it can be seen that Fe and Al were removed as hydroxides with varying pH gradients. Though co-precipitation might have happened, Fe and Al were mainly removed as hydroxides. This further confirms the XRD and TEM-EDS results.

Table 2
Calculation of Saturation Index (SI) for selected mineral phases at various pH.

Mineral phase	pH								
	2	3	3	3	5	8	8	9	10
$Al(OH)_3(a)$	−10	−6.9	−7	−6	0	0	0	0	0
Alunite	−8	−2.4	−2	−1	11.21	2.74	2.3	1.77	−0.29
Anhydrite	−0.4	0	0.2	1	0.47	0.56	0.63	0.68	0.73
$Fe(OH)_3(a)$	−2.7	0	0	0	0	0	0	0	0
Gibbsite	−6.8	−4	−4	−3	2.84	2.84	2.84	2.84	2.84
Goethite	2.6	5	5	5	5.3	5.3	5.3	5.3	5.3
Gypsum	0.1	0.5	1	0.83	0.94	1.04	1.1	1.16	−13.31
Hausmannite	−36	−29	−29	−28.56	−24.31	−18.64	−18	−17.07	1.21
Hematite	7.1	13	13	12.52	12.52	12.52	12.52	12.52	12.52
Jarosite-K	0.4	6	6	5.15	−1.21	−9.67	−10.12	−10.65	−12.71

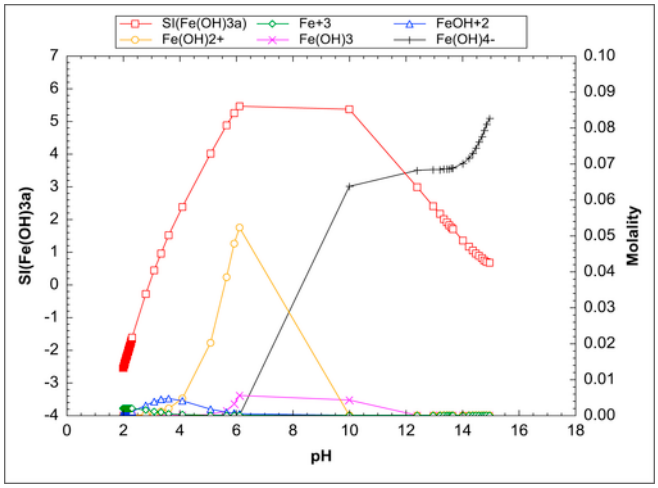

Fig. 9. PHREEQC modelled chemical species concentration of BOF slag treated coal mine water.

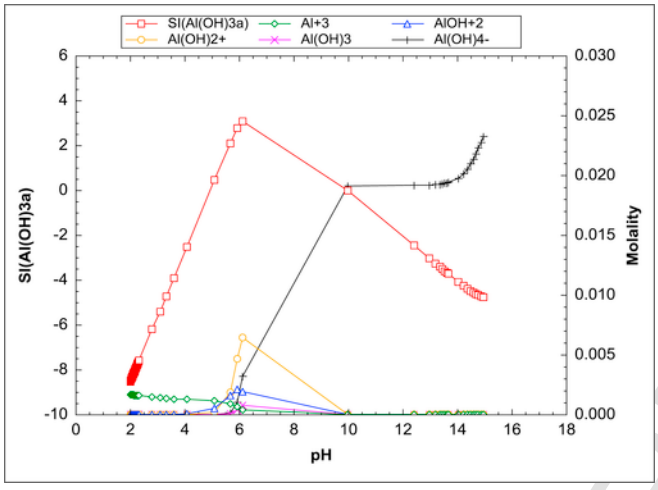

Fig. 10. PHREEQC modelled chemical species concentration of BOF slag treated coal mine water.

5. Water quality of feed AMD and BOF slag reacted AMD

Chemical compositions of AMD before and after contacting BOF slag are shown in Table 3.

As shown in Table 3, the pH of coal mine water used in this study was 2 and it was increased to 10 after contacting the BOF slag. Alkalinity was recorded to be ≤ 5 mg/L before contacting the coal mine water and 11 mg/L after contacting coal mine water. Alkalinity was expressed as $CaCO_3$. Total dissolved solids (TDS) and electrical conductivity (EC) of the supernatant solution were recorded to have decrease from 28000 to 6500 mg/L and from 1000 to 240 mS/cm respectively. High TDS and EC are is attributed to large quantity of dissolved metal species and sulphates. The reduction in TDS and EC is attributed to chemical species attenuation. The water hardness also went up, this may be attributed to an increase in the concentration of Magnesium and Calcium when BOF slag is dissolving. The sulphate recorded in this sample was 8000 mg/L hence making this anion dominant in aqueous solution. This is suitable for commercial gypsum recovery. Major cations included Fe, Al, Mn, Ca, Mg, K and traces of Cu, Co, Pb, Ni, Zn and Cd. Insignificant amount of

Table 3
Chemical profile of raw coal AMD, BOF reacted-AMD and DWS/SANS water quality standards.

Parameters	AMD	BOF	Units	DWS/SANS standards
Alkalinity $CaCO_3$	<5.0 ± 1	11 ± 0.5	mg/L	≤120
Aluminium	480 ± 0.1	<0.70 ± 0.01	mg/L	≤300
Cadmium	10 ± 0	<0.20 ± 0	mg/L	≤3
Calcium	470 ± 0	840 ± 0	mg/L	≤300
Cobalt	30 ± 0.4	<0.35 ± 0.9	mg/L	≤0.2
Copper	1 ± 1	<0.40 ± 0.1	mg/L	≤2000
Electrical Conductivity	1000 ± 0.9	470 ± 0.5	mS/cm	≤170
Fluoride	<0.20 ± 1	<0.20 ± 1	mg/L	≤1.5
Iron	6000 ± 1	<0.90 ± 1	mg/L	≤300
Lead	5 ± 1.5	<0.10 ± 0.09	mg/L	≤10
Magnesium	480 ± 0.05	720 ± 1.4	mg/L	≤400
Manganese	130 ± 0.5	15 ± 4	mg/L	≤100
Nickel	30 ± 0.6	<0.40 ± 0.2	mg/L	≤70
pH	2 ± 0.7	10 ± 0.05	–	≥5 to ≤9.7
Potassium	2 ± 1.5	9.5 ± 1	mg/L	≤20
Silicon	30 ± 0.01	1.5 ± 0.04	mg/L	≤6
Sodium	30 ± 1.3	55 ± 1	mg/L	≤200
Sulphate	8000 ± 0.31	400 ± 2.1	mg/L	≤500
Total Dissolved solids	28000 ± 0.6	6500 ± 1.7	mg/L	≤1200
Total Hardness	3100 ± 0.5	5100 ± 1.5	mg/L	–
Zinc	20 ± 0.05	<0.60 ± 0.95	mg/L	≤5

chromium was determined to be present in the BOF slag matrices. The predominance of Fe and SO_4^{2-} indicated that this mine water was subjected to pyrite oxidation. The presences of base cations (K, Na, Mg, Al and Ca) may be attributed to the dissolution of silicate minerals such as feldspar, kaolinite, and chlorite. Traces of sulphide bearing minerals such as Cu, Co, Pb, Ni, Zn and Cd were also observed to be present at minute concentration. After the reaction chemistry, only TDS, EC, Ca, Mg and sulphate were observed to be above the prescribed limit as stipulated by the water quality guidelines. PHREEQC geochemical model predicted Mg to be under saturated. Mg species form relatively $MgSO_4$ complex in solution hence are expected to remain largely in solution. These may be some of the reasons why sulphate was not removed completely from the solution. Though above the limit, calcium was reduced significantly and it was predicted to precipitate as gypsum, calcite and dolomite. The simulations showed that in the feed water, Fe existed mainly as Fe^{2+} and Fe^{3+} while the rest of the metals, except for Na and K, were in their divalent states at acidic solution. From these results, the treated water is suitable for agricultural use, discharge purposes and industrial reuse.

6. Conclusions

This study further validated that BOF slag can be used for the treatment of very acidic, and metalliferous mine water. Reaction of BOF slag and coal mine water led to an increase in pH (≥10) and a significant reduction in inorganic species concentrations. Attenuation of sulphate, Al, Mn, Fe and other chemical species was observed to be optimum at 60 min of agitation at S: L ratio of 1 g: 100 mL. Under these conditions, the pH achieved was ≥10, which is suitable enough for metal removal. From PHREEQC geochemical modelling, it was predicted that most chemical species formed sulphate-bearing minerals and the formation of those mineral phases follow a selective and fractional precipitation sequence that has Fe^{3+} at pH ˃ 6, Al^{3+} at pH ˃ 6, Fe^{2+} at pH ˃ 8, Mn^{2+}, Ca^{2+} and Mg^{2+} at pH ˃10. This sequence implied that it would be possible to pursue fractional precipitation with separate precipitates of various metals, making this technology viable for instances where the commercial value of the recovered metals are being pursued. XRF and XRD results were in agreement with

PHREEQC geochemical model. This study has further verified that BOF slag has the potential of neutralizing the acidity of AMD and attenuating toxic chemical species. Moreover, gypsum and magnetite were also recovered from the mine water treatment process using BOF slag hence indicating that there is a commercial value from this water treatment process. A disadvantage of this technology is that most of the alkali, alkaline earth metals and sulphate remained in solution which means a polishing technology such as reverse osmosis (RO) need to be coupled to produce drinking water quality. As such, this study recommends the coupling of RO process to this technology to produce water of drinking standard.

Acknowledgements

The authors wish to express their sincere gratitude to the Council for Scientific and Industrial research (CSIR) and City of Johannesburg for providing financial support to this project. Furthermore, the authors would like to thanks Corlien Cloete from CGS for XRF analysis, Charity Maepa for HR-SEM analysis, Tshwane University of Technology for providing lab space to execute this research work. The authors would also like to thank Khathutshelo Muedi for the helpful and insightful discussions.

References

Akinwekomi, V., Maree, J.P., Zvinowanda, C., Masindi, V., 2017. Synthesis of magnetite from iron-rich mine water using sodium carbonate. J. Environ. Chem. Eng.

Aziz, M.M.A., Hainin, M.R., Yaacob, H., Ali, Z., Chang, F.L., Adnan, A.M., 2014. Characterisation and utilisation of steel slag for the construction of roads and highways. Materials Research Innovations. 18, S6-255-S256-259.

Belhadj, E., Diliberto, C., Lecomte, A., 2012. Characterization and activation of basic oxygen furnace slag. Cem. Concr. Compos. 34, 34–40.

Bodurtha, P., Brassard, P., 2000. Neutralization of acid by steel-making slags. Environ. Technol. 21, 1271–1281.

Bologo, V., Maree, J.P., Carlsson, F., 2012. Application of magnesium hydroxide and barium hydroxide for the removal of metals and sulphate from mine water. Water sa. 38, 23–28.

Chen, Z., Wu, S., Xiao, Y., Zeng, W., Yi, M., Wan, J., 2016. Effect of hydration and silicone resin on Basic Oxygen Furnace slag and its asphalt mixture. J. Clean. Prod. 112, 392–400.

Chen, Z., Xie, J., Xiao, Y., Chen, J., Wu, S., 2014. Characteristics of bonding behavior between basic oxygen furnace slag and asphalt binder. Constr. Build. Mater. 64, 60–66.

Chiou, C.-S., Chang, C.-F., Chang, C.-T., Shie, J.-L., Chen, Y.-H., 2006. Mineralization of Reactive Black 5 in aqueous solution by basic oxygen furnace slag in the presence of hydrogen peroxide. Chemosphere 62, 788–795.

Clyde, E.J., Champagne, P., Jamieson, H.E., Gorman, C., Sourial, J., 2016. The use of a passive treatment system for the mitigation of acid mine drainage at the Williams Brothers Mine (California): pilot-scale study. J. Clean. Prod. 130, 116–125.

Doye, I., Duchesne, J., 2003. Neutralisation of acid mine drainage with alkaline industrial residues: laboratory investigation using batch-leaching tests. Appl. Geochem. 18, 1197–1213.

Du, Y., Lu, Q., Chen, H., Du, Y., Du, D., 2016. A novel strategy for arsenic removal from dirty acid wastewater via CaCO3-Ca(OH)2-Fe(III) processing. J. Water Process Eng. 12, 41–46.

Gitari, M., Petrik, L., Etchebers, O., Key, D., Iwuoha, E., Okujeni, C., 2006. Treatment of acid mine drainage with fly ash: removal of major contaminants and trace elements. J. Environ. Sci. Health - Part A Toxic/Hazardous Subst. Environ. Eng. 41, 1729–1747.

Goetz, E.R., Riefler, R.G., 2014. Geochemistry of CO2 in steel slag leach beds. Mine Water Environ.

Hallberg, K.B., 2010. New perspectives in acid mine drainage microbiology. Hydrometallurgy 104, 448–453.

Hammarstrom, J.M., Sibrell, P.L., Belkin, H.E., 2003. Characterization of limestone reacted with acid-mine drainage in a pulsed limestone bed treatment system at the Friendship Hill National Historical Site, Pennsylvania, USA. Appl. Geochem. 18, 1705–1721.

Jafaripour, A., Rowson, N.A., Ghataora, G.S., 2015. Utilisation of residue gas sludge (BOS sludge) for removal of heavy metals from acid mine drainage (AMD). Int. J. Miner. Process. 144, 90–96.

Lee, W.-C., Lee, S.-W., Yun, S.-T., Lee, P.-K., Hwang, Y.S., Kim, S.-O., 2016. A novel method of utilizing permeable reactive kiddle (PRK) for the remediation of acid mine drainage. J. Hazard. Mater. 301, 332–341.

Madzivire, G., Gitari, W.M., Vadapalli, V.R.K., Ojumu, T.V., Petrik, L.F., 2011. Fate of sulphate removed during the treatment of circumneutral mine water and acid mine drainage with coal fly ash: modelling and experimental approach. Miner. Eng. 24, 1467–1477.

Madzivire, G., Petrik, L.F., Gitari, W.M., Ojumu, T.V., Balfour, G., 2010. Application of coal fly ash to circumneutral mine waters for the removal of sulphates as gypsum and ettringite. Miner. Eng. 23, 252–257.

Mahieux, P.Y., Aubert, J.E., Escadeillas, G., 2009. Utilization of weathered basic oxygen furnace slag in the production of hydraulic road binders. Constr. Build. Mater. 23, 742–747.

Manchisi, J., Rowson, N.A., Simmons, M.J.H., 2013. Kinetics of metals adsorption in acid mine drainage treatment with blast furnace slag. 23rd International Mining Congress and Exhibition of Turkey. IMCET 2013, 1803–1813.

Maree, J.P., Mujuru, M., Bologo, V., Daniels, N., Mpholoane, D., 2013. Neutralisation treatment of AMD at affordable cost. Water SA. 39, 245–250.

Masindi, V., 2016. A novel technology for neutralizing acidity and attenuating toxic chemical species from acid mine drainage using cryptocrystalline magnesite tailings. J. Water Process Eng. 10, 67–77.

Masindi, V., Gitari, M.W., Tutu, H., De Beer, M., 2016. Fate of inorganic contaminants post treatment of acid mine drainage by cryptocrystalline magnesite: complimenting experimental results with a geochemical model. J. Environ. Chem. Eng. 4, 4846–4856.

Masindi, V., Gitari, M.W., Tutu, H., Debeer, M., 2017. Synthesis of cryptocrystalline magnesite–bentonite clay composite and its application for neutralization and attenuation of inorganic contaminants in acidic and metalliferous mine drainage. J. Water Process Eng. 15, 2–17.

Mikhail, S.A., Turcotte, A.-M., 1998. Thermal reduction of steel-making secondary materials: I. Basic-oxygen-furnace dust. Thermochim. Acta 311, 113–119.

Name, T., Sheridan, C., 2014. Remediation of acid mine drainage using metallurgical slags. Miner. Eng. 64, 15–22.

Oluwasola, E.A., Hainin, M.R., Aziz, M.M.A., 2014. Characteristics and utilization of steel slag in road construction. J. Teknol. 70, 117–123.

Parkhurst, D.L., Appelo, C. a. J., 1999. Users guide to Phreeqc (Version 2) - a computer program for speciation, batch-reactions, one-dimensional transport and inverse geochemical calculations. Water-Resour. Investig. Rep. 99–4259.

Petrik, L.F., White, R.A., Klink, M.J., Somerset, V.S., Burgers, C.L., Fey, M.V., 2003. Utilization of South African fly ash to treat acid coal mine drainage, and production of high quality zeolites from the residual solids. In: Proceedings of the 2003 International Ash Utilisation Symposium.

Pozo-Antonio, S., Puente-Luna, I., Lagüela-López, S., Veiga-Ríos, M., 2014. Techniques to correct and prevent acid mine drainage: a review. DYNA Colomb. 81, 73–80.

Rajendran, K., Balakrishnan, G.S., Kalirajan, J., 2015. Synthesis of magnetite nanoparticles for arsenic removal from ground water pond. Int. J. PharmTech Res. 8, 670–677.

Reddy, A.S., Pradhan, R.K., Chandra, S., 2006. Utilization of Basic Oxygen Furnace (BOF) slag in the production of a hydraulic cement binder. Int. J. Miner. Process. 79, 98–105.

Sahinkaya, E., Gungor, M., 2010. Comparison of sulfidogenic up-flow and down-flow fluidized-bed reactors for the biotreatment of acidic metal-containing wastewater. Bioresour. Technol. 101, 9508–9514.

Sahinkaya, E., Gungor, M., Bayrakdar, A., Yucesoy, Z., Uyanik, S., 2009. Separate recovery of copper and zinc from acid mine drainage using biogenic sulfide. J. Hazard. Mater. 171, 901–906.

Simmons, J., Ziemkiewicz, P., Black, D.C., 2002. Use of steel slag leach beds for the treatment of acid mine drainage. Mine Water Environ. 21, 91–99.

Tutu, H., Cukrowska, E.M., Mccarthy, T.S., Hart, R., Chimuka, L., 2009. Radioactive disequilibrium and geochemical modelling as evidence of uranium leaching from gold tailings dumps in the Witwatersrand Basin. Int. J. Environ. Anal. Chem. 89, 687–703.

Wei, X., Viadero Jr., R.C., 2007. Synthesis of magnetite nanoparticles with ferric iron recovered from acid mine drainage: implications for environmental engineering. Colloids Surfaces A Physicochem. Eng. Aspects 294, 280–286.

Wei, X., Viadero Jr., R.C., Buzby, K.M., 2005. Recovery of iron and aluminum from acid mine drainage by selective precipitation. Environ. Eng. Sci. 22, 745–755.

Xue, Y., Wu, S., Hou, H., Zha, J., 2006. Experimental investigation of basic oxygen furnace slag used as aggregate in asphalt mixture. J. Hazard. Mater. 138, 261–268.

Yesilnacar, M.I., Kadiragagil, Z., 2013. Effects of acid mine drainage on groundwater quality: a case study from an open-pit copper mine in eastern Turkey. Bull. Eng. Geol. Environ. 72, 485–493.

Zvimba, J.N., Siyakatshana, N., Mathye, M., 2017. Passive neutralization of acid mine drainage using basic oxygen furnace slag as neutralization material: experimental and modelling. Water Sci. Technol. 75, 1014–1024.